A Simple Auxiliary Model for Field Amplitude Shaping in Complex Environments, and Application to MRI Shimming

SABRINA ZUMBO[1], TOMMASO ISERNIA [1,2,3] (Fellow, IEEE), AND MARTINA TERESA BEVACQUA [1,3] (Member, IEEE)

[1]Dipartimento di Ingegneria dell'Informazione, delle Infrastrutture e dell'Energia Sostenibile, Università Mediterranea di Reggio Calabria, 89124 Reggio Calabria, Italy

[2]CNR, Istituto per il Rilevamento Elettromagnetico dell'Ambiente, CNR-IREA, 80100 Naples, Italy

[3]Consorzio Nazionale Interuniversitario per le Telecomunicazioni, 43124 Parma, Italy

CORRESPONDING AUTHOR: M. T. BEVACQUA (e-mail: martina.bevacqua@unirc.it)

ABSTRACT The canonical problem of designing the complex excitations feeding an array such to ensure a desired field intensity distribution inside a given region of interest, while keeping it under control in some other regions, is addressed. To this end, an auxiliary physics inspired model for the induced total field is proposed, whose off-line analysis allows a simplified approach to understand the convenient and non-convenient field interferences between canonical solutions for the induced total field, that are zero order Bessel functions. Moreover, its analysis drastically reduces the computational burden associated to the *multi-control* points based approaches. The problem at hand plays a key role in many different applications, including radio communications, wireless power transfer as well as hyperthermia treatment planning, and in this paper attention is paid to radiofrequency shimming in magnetic resonance imaging. In fact, the proposed model and tools are tailored to the challenging case of leveling of the magnetic field intensity within an MRI scanner and in case of a bidimensional realistic head phantom.

INDEX TERMS Antenna array, electromagnetic field, inverse problem, intensity shaping, magnetic resonance imaging, shimming.

I. INTRODUCTION

A BASIC problem in wave physics and in applied electromagnetics is to generate a field intensity distribution with some desired characteristics in a specific region of interest (ROI), such as f.i. intensity, uniformity, sidelobes levels. This problem is relevant in a wide range of applications, including antenna synthesis for radar and communications [1], [2], energy replenishment [3], [4], through-the-wall imaging [5], and biomedical applications [6]–[8]. As far as these latter are concerned, field intensity shaping plays a key role in hyperthermia treatment planning, wherein one aims to increase the temperature inside a tumor by means of a proper antenna array applicator, while keeping under control the

heating in the surrounding healthy tissues [6]. Also, one of the main challenges for magnetic resonance imaging (MRI) at high and ultra-high fields is the radiofrequency shimming, which consists in ensuring a significant homogeneity of the transmit magnetic field in the anatomical region to be imaged, while guaranteeing the specific absorption rate (SAR) limits in the patient body [7]. Notably, the ability to arbitrarily shape the field intensity is really challenging when the ROI is a highly inhomogeneous medium, as in case of hyperthermia or radiofrequency MRI shimming at high field.

All the above applications imply the proper shaping of the field intensity in a given ROI. Many different strategies have been developed for the case of fixed

geometry arrays to find the optimal antenna array excitations that guarantee the desired field shape. As the problem is intrinsically non-convex, the issue of the possible occurrence of sub-optimal solutions arises. Indeed, if local optimization procedures are adopted, one could be trapped in local minima, which represent *false* and suboptimal solutions of the problem. Instead, in case of global optimization procedures, the involved computation burden rapidly increases for large number of unknown. Then, in both cases, the globally optimal solution cannot be generally guaranteed.

In such a contest, a very recent paradigm is the one proposed in [9], [10] wherein the phase shifts between the fields at specific *control* points, which are properly located over the ROI, are assumed as auxiliary unknown variables of the problem. This recent paradigm has shown good performance in the synthesis of generic array for telecommunications [11] and hyperthermia [12]. However, since the optimal phase shifts are not a priori known, one has to determine it by exploring the set of possible phase shifts using enumerative or global optimizations. As a consequence, the computational burden grows rapidly if the number of *control* points increases, and this circumstance may prevent the use of this paradigm in a number of actual applications.

In this paper, a simple auxiliary and physics inspired model for the induced total field is proposed for shaping the field intensity. The model allows a relatively simple physical understanding of convenient and non-convenient fields interferences to be exploited in the shaping problem, and hence a drastic reduction of the computational burden related to its solution via optimization procedure. In particular, it allows to obtain in an easy fashion convenient field distributions within the ROI that one can fit to address the shaping problem. Also, in those cases where stringent shaping constraints are present, the use of the auxiliary model allows a significant resize of the set of possible phase shifts to be considered in approaches [9], [10].

Besides presenting the new auxiliary model, we test it against MRI shimming [7], which consists in avoiding as much as possible inhomogeneities in the RF magnetic field, as they are causes of image degradation. Then, the auxiliary model is applied to the challenging case of leveling of the magnetic field intensity within an MRI scanner, wherein, differently from applications and shaping approaches in [9]–[12], the magnetic field amplitude distribution is of interest.

The paper is organized as follows. In Section II, we briefly summarize the basic mathematical formulation of a generic shaping problem. In Sections III and IV, the proposed auxiliary model for the induced total field is described and analyzed in a homogeneous medium. Finally, in Sections V and VI, MRI shimming is considered and the proposed field model tested against a 2D realistic head phantoms. Then, conclusions follow.
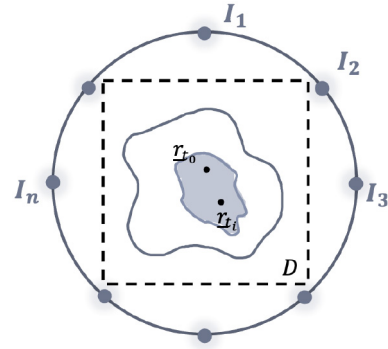

FIGURE 1. Sketch of the scenario under test. The ROI is the grey area and contains the control points, indicated by black points. N elementary monochromatic electric sources, indicated by grey circles, surround the investigation domain D.

II. STATEMENT OF THE PROBLEM

Assume that the geometry as well as the electromagnetic properties of the bidimensional scenario under test D wherein the ROI is embedded (i.e., relative permittivity $\epsilon_r(r)$ and electric conductivity $\sigma(r)$), are known. Moreover, consider N elementary monochromatic sources surrounding D and that one of the electromagnetic field components is dominant above the other ones or that the optimal/desired polarization of the electromagnetic field distribution is a priori known. With the reference to the 2D scheme in Figure 1 and indicating with $\underline{r} = (x, y)$ a generic point of D, the overall dominant electric E and magnetic B field components can be expressed as:

$$B(\underline{r},\ I_n) = \sum_1^N I_n b_n(\underline{r}), \tag{1a}$$

$$E(\underline{r}, I_n) = \sum_1^N I_n e_n(\underline{r}), \tag{1b}$$

wherein (e_n, b_n) are the total electric and magnetic fields induced by the unitary excited n-th element when all the other elements are off, while $I_n(n = 1, 2, \ldots, N)$ are the complex excitation coefficients.

Then, the optimization shaping problem can be formulated as follows:

> "*Determine the optimal set of complex excitations coefficients I_n such to produce the desired behavior of the amplitude of the given field component in the ROI, while enforcing some constraints in other regions of D*".

To be more specific, one usually aims to maximize the amplitude of the field as well as ensuring its uniformity in the ROI. This is the case of microwave hyperthermia or MRI shimming. Instead, SAR limits or other kind of upper bounds are usually enforced in the whole D or in $D\backslash ROI$. Unfortunately, these requirements involve the solution of a non-convex problem. Hence, by using local as well as global optimization procedures, because of the involved

computation burden for large N, the global optimality of the solution cannot be generally ensured.

In the following, an effective physics inspired model is proposed for the total induced field in order to understand convenient and non-convenient fields interferences to be exploited in the shaping problem.

III. AN AUXILIARY FIELD MODEL FOR AMPLITUDE SHAPING

In the relevant paper of Woodward and Lawson [13], the far field shaping problem has been tackled by looking for a superposition of many patterns focused in properly chosen given points located in the ROI. However, in [13] one cannot enforce any constraints outside the target area and the single focused patterns are simply added in phase without considering any possible phase shifts.

Starting from the above, an interesting possibility for the solution of the shaping problem is that of considering an auxiliary field model wherein the shaping is tackled as the superposition of single patterns focused in a number of points, called *control* point $\underline{r}_{t_i}$, inside the ROI. Interestingly, the combinations of these single focused bricks involve additional degrees of freedom, which are missing in [13], i.e., the phases of the field in $\underline{r}_{t_i}$. These latter, and a proper choice of the control points, will allow to control to some extent the field intensity in the ROI.

Along this line of reasoning, and considering for the time being a 2D homogeneous region of space, the field of interest in the neighborhood of the control point $\underline{r}_{t_i}$, denoted as $F_i(\underline{r})$, can be expressed in a reference system centered on $\underline{r}_{t_i}$ as a superposition of basic solutions as [14]:

$$F_i(\underline{r}) = \sum_{\ell=-\infty}^{+\infty} a_\ell J_\ell(k_m|\underline{r} - \underline{r}_{t_i}|)e^{j\ell\angle(\underline{r}-\underline{r}_{t_i})} \quad (2)$$

where a_ℓ is an amplitude coefficient, $J_\ell(\cdot)$ is the Bessel function of order ℓ, k_m is the wave number in the ROI and $\angle(\underline{r} - \underline{r}_{t_i})$ is the angle in polar coordinates with respect to $\underline{r}_{t_i}$, in a bidimensional system.

Whenever such a field is focused in $\underline{r}_{t_i}$, the only term which survives is the one for $\ell = 0$. As a consequence, in such a case $F_i(\underline{r})$ can be approximated, apart from the constant a_0, by means of the zero order Bessel function J_0, which is centered in the control point $\underline{r}_{t_i}$.

Then, suppose that the desired shaped field is a superposition of fields focused in the different control points, and, in view of our final goals, that the different focused components have all the same amplitude $a_0 = 1^1$. Then, apart from a single unessential constant, the field can be approximated as:

$$F_{aux}(\underline{r}) = J_0(k_m|\underline{r} - \underline{r}_{t_0}|) + \sum_{i=1}^{L} J_0(k_m|\underline{r} - \underline{r}_{t_i}|)e^{j\phi_i} \quad (3)$$

1. By the sake of simplicity, we are herein reasoning on a 'flat top' kind of shaping. Differently weighted superpositions can be considered in other cases.

where $\phi_i \in [0, 2\pi[$ are auxiliary variables indicating the phase of the different Bessel functions addenda in the auxiliary model (3).

Provided the simplification of relation (2) is adequate for the original shaping problem at hand, the analysis of model (3) can allow a relatively simple physical understanding of convenient and non-convenient Bessel-field interferences determined from $\{\phi_i\}$ values. For example, in case of just two control points, a π value of ϕ_1 would imply a null of the field $F_{aux}(\underline{r})$ at midway, so that such a value and the neighbouring ones can be discarded if a uniform amplitude field is required within the ROI. This is of course true even if in expression (3) no other constraints are taken into account outside the 'flat-top' zone. In fact, values of ϕ_1 implying a null of the field $F_{aux}(\underline{r})$ at midway certainly are not of interest and can be discarded in the solution of the relevant shaping problem. Interestingly, in the same two control points case and uniformity requirement, one can also analytically determine a value of ϕ_1 such that the auxiliary fields have the same amplitude at the external points and at midway. In case of lossless media, such an optimal value is readily found as discussed in the Appendix.

Then, although the cases with three or more control points are more and more difficult to be analysed, model (3) can give very useful insights about possible field interferences when varying $\{\phi_i\}$ values, and hence useful guidelines for an optimal solution of the shaping problem, as discussed below.

In fact, the auxiliary problem of determining the more convenient set of values for $\{\phi_i\}$ has a series of convenient characteristics as follow:

1) because of the simple analytical form (3), one can indagate in a very fast fashion many $\{\phi_i\}$ values combinations, without solving any optimization problem or other additional procedures as in [9]–[12];
2) for the same reason, its repeated analysis also can possibly give suggestions on the selection of the control points $\underline{r}_{t_i}$;
3) results arising from extensive investigation of model (3) by varying $\{\phi_i\}$ values (and eventually also the distances $|\underline{r} - \underline{r}_{t_i}|$) can be arranged into a Pareto like performance plot, giving back the more convenient ranges of the phase shifts combinations;
4) these results have a wide range of validity and can be adopted to a large series of cases, sharing the same electrical distances amongst the control points, even when k_m is an average value of the wavenumber in a non-homogeneous scenario (see Section VI).

In summary, the auxiliary model (3) can be profitably exploited to identify convenient and non-convenient $\{\phi_i\}$ values. Once L control points are set in the ROI (step 1 in Figure 2), the performance parameters $(PP_1, PP_2, \ldots PP_n)$ are defined depending on the application at hand (step 2 in Figure 2). Possible choices are the ripple and the average value in the ROI, but different choices are indeed possible. In order to explore all possible ϕ_i values, M samples
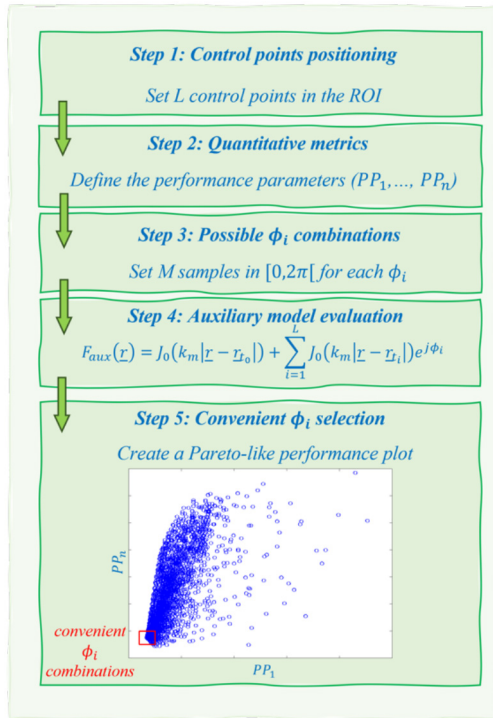
FIGURE 2. Schematic flowchart of the analysis procedure of the auxiliary model (3).

in $[0, 2\pi[$ are set for each ϕ_i and M^{L-1} combinations are considered (step 3 in Figure 2). Then, $F_{aux}(\underline{r})$ is evaluated by Equation (3) for each $\{\phi_i\}$ combination (step 4 in Figure 2) and, hence, those combinations corresponding to the worse performance are discarded. Also, the $\{\phi_i\}$ combinations which corresponds to the optimal values of the performance indicators PP_n are selected. To this end, it comes out to be convenient to report the indicators PP_n in a Pareto like performance plot (step 5 in Figure 2).

A scheme of the analysis procedure is resumed in the flowchart of Figure 2. At the end of the procedure, the analysis of the Pareto-like performance plot allows to easily identify the $\{\phi_i\}$ combinations to be discarded as well as the more convenient ones. For example, if performance parameters PP_n are defined in such a way that better performance are obtained when they assume low values, the low-left corner points correspond to the more convenient $\{\phi_i\}$ combinations (see f.i. the red box in Figure 2).

As far as step 1 is concerned, it is important to note that the overall strategy amounts to find some appropriate interferences amongst different elementary bricks, herein given by Bessel functions. Hence, in order to have eventually significant interferences, the distance amongst two control points has to be such that the elementary bricks are not too small in the ROI, or at least along the line joining the two points. On the other hand, very small distances among the control points also do not have sense, as the control points would be redundant and this circumstance would just increase the computational burden, without adding useful information. As a rule of thumb deriving from an extensive numerical analysis (a part of it reported in Section IV), distances belonging to the interval $[0.25, 0.5]\lambda_b$ are suggested. As a second possibly useful comment, note that within this interval, the simplicity of the proposed auxiliary model allows one also to understand what is the best location distance. In fact, one could select the distance implying a minimum RSD and a maximum field amplitude, according to the analysis resumed in Figure 2. Finally, an additional criterion for choosing the position of the control points is the need of covering in a possibly uniform fashion the region of interest.

The analysis shown in the Figure 2, allows two effective possibilities for the solution of the relevant shaping problem. First, understanding the optimal field interferences also implies achieving convenient field distributions within the ROI. Then, in order to solve the actual problem of determining the complex excitations of the primary sources, one can simply minimize the misfit between the actual field distribution (1) and the reference target distribution(s) as determined from the above analysis. Notably, this is indeed a field synthesis problem which can be easily solved by the minimization of a quadratic functional.

Second, once one has gained awareness of convenient and non-convenient interferences, one can take advantage of such a knowledge within a constrained power optimization framework. In particular, as it will be discussed in detail in the numerical analysis in Section VI, the outcomes of model (3) can play a pivotal role in *multi-control points*-based approaches [9]–[12], as it allows time and memory saving in the overall optimization, without affecting the final performance.

IV. ANALYSIS OF THE AUXILIARY FIELD MODEL

In order to give a better insight into the auxiliary model (3), in this section a numerical analysis is reported in the simple case of homogeneous medium. In particular, the analysis procedure in Figure 2 is performed. The aim of the shaping problem at hand is to achieve a uniform and intense amplitude field distribution within a given ROI. As far as the check of the usefulness of this analysis in a relevant actual shaping problem is concerned, the reader is deferred to Sections V and VI, wherein application to the challenging MRI shimming case is considered.

In the following two subsections, a square domain of side $L = 0.76\lambda_b$ is considered, discretized into $N_x \times N_y$ small cells, with $N_x = N_y = 80$, where λ_b is the wavelength in a homogenous medium with relative permittivity of 53 and electrical conductivity 0.15. The working frequency is 128MHz.

As expected, expression (3) tuns out to be exact for the case of a single control point, i.e., for the focusing problem. More interestingly, the Bessel function of zero order comes out to be quite accurate to approximate the spatial distribution of the focused field in a neighborhood of the control
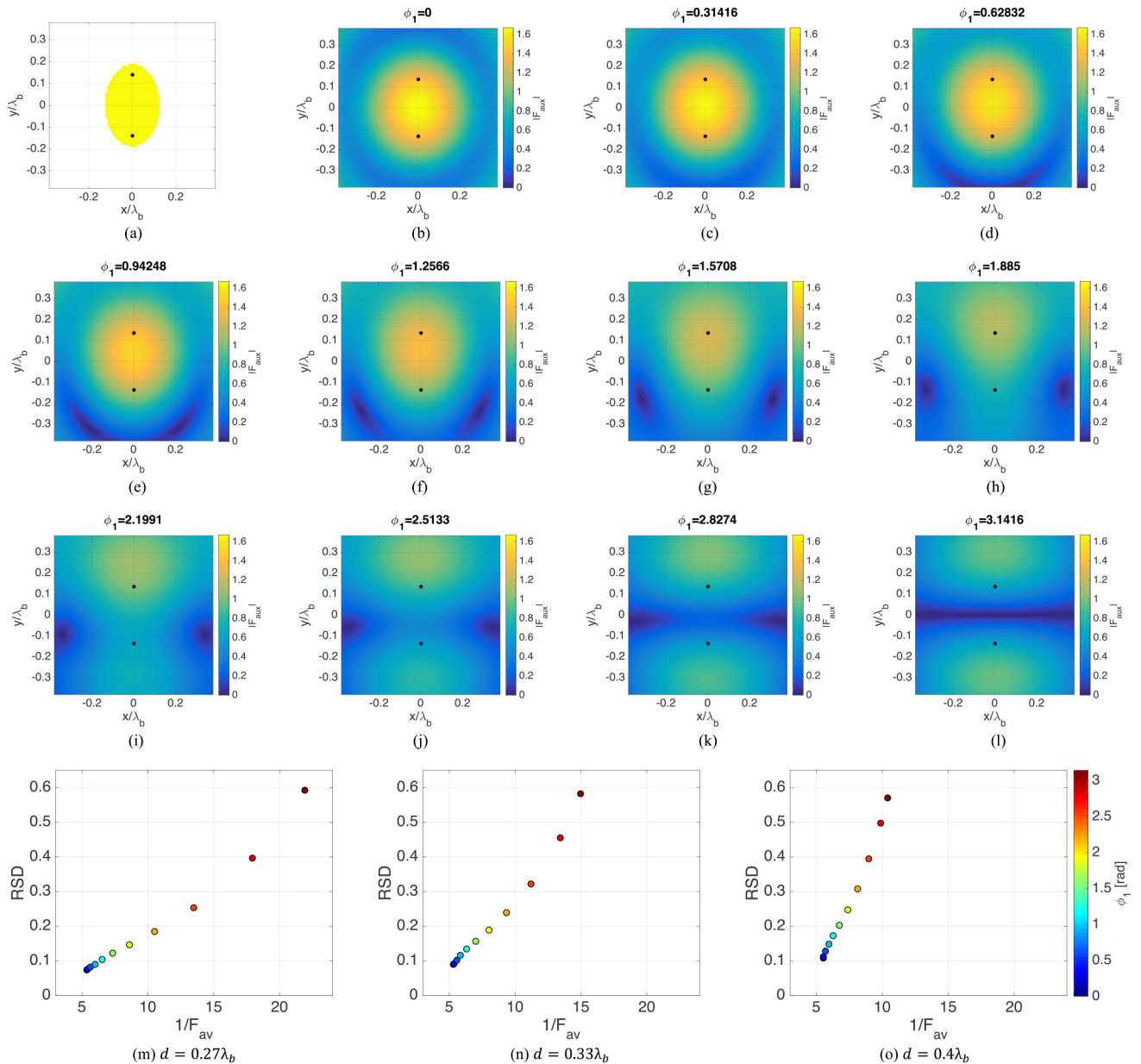
FIGURE 3. Analysis of the auxiliary field model. CASE STUDY 1. (a) Scenario under test. The ROI is the yellow area, while the control points are superimposed as black points at distance $d = 0.27\lambda_b$. (b)-(l) Spatial amplitude distributions of the auxiliary field model for different values of phase shifts in $[0,\pi]$ for $d = 0.27\lambda_b$. RSD versus the reciprocal of F_{av} for (m) $d = 0.27\lambda_b$, (n) $d = 0.33\lambda_b$ and (o) $d = 0.4\lambda_b$. Each circle represents a pair of values (RSD, $1/F_{av}$) corresponding to a given phase shift in the interval $[0,\pi]$.

point even in the case of a non-homogeneous scenario (see Section VI below).

In the two subsections which follow the analysis of model (3) for the cases of two and four control points is in order.

A. CASE STUDY 1: TWO CONTROL POINTS

The scenario under test is depicted in Figure 3(a). The control points are located at a distance $d = 0.27\lambda_b$. The midpoint is at (0,0) m. The ROI is represented by the yellow ellipse in Figure 3(a).

According to step 3 in Figure 2, M = 20 values of ϕ_1 have been uniformly sampled in $[0, 2\pi]$. The spatial

distributions of the auxiliary field amplitude obtained by considering 11 values of ϕ_1 evenly spaced in $[0, \pi]$ are shown in Figure 3. The same results are obtained in case of $\phi_1 \in]\pi, 2\pi[$. Note that, by virtue of the simple analytical form of (3), its evaluation for different ϕ_1 values is immediate. As expected, when ϕ_1 approaches π a disruptive interference arises between the two Bessel functions. Instead, for phase shifts near to 0 (or 2π), a satisfactory tradeoff between amplitude and uniformity is obtained. Note that these results are also in agreement with the examples in Figure 3 of paper [10].

In order to evaluate in a systematic way the optimal phase shift ϕ_1 able to both ensure a uniform and intense
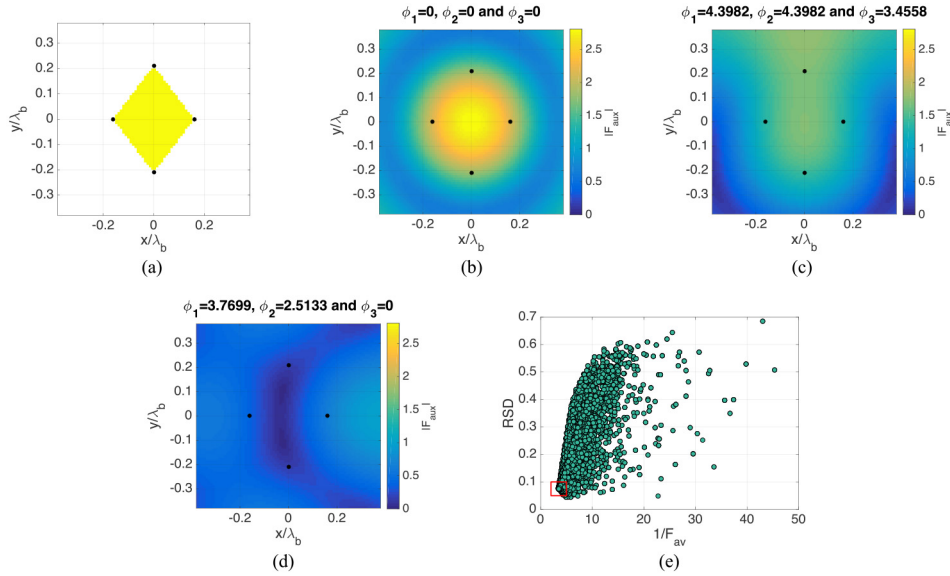
FIGURE 4. Analysis of the auxiliary field model. CASE STUDY 2. (a) Scenario under test. The ROI is the yellow area, while the control points are superimposed as black points at distances $d_{01} = 0.42\lambda_b$ and $d_{23} = 0.32\lambda_b$. Spatial amplitude distributions of the auxiliary field model in case of (b) good tradeoff between RSD and maximum auxiliary field intensity in the ROI, (c) minimum RSD and (d) maximum RSD. (e) RSD versus the reciprocal of F_{av}. Each green circle represents a pair of values (RSD, $1/F_{av}$) corresponding to a given combination of phase shifts. The red box delimits the region corresponding to the best tradeoff between minimum RSD and maximum F_{av}.

spatial distribution of the field intensity, we consider two quantitative synthetic performance indicators. In particular, we consider the average value of the field intensity F_{av} and the relative standard deviation of the amplitude (RSD), defined as:

$$RSD = \frac{std\{|F|\}}{mean\{|F|\}} \quad (4)$$

being $std\{\cdot\}$ and $mean\{\cdot\}$ respectively the standard deviation and the mean. Both indicators are evaluated within the ROI. Performance is easily evaluated in case of different distances between the control points. In particular, in Figures 3(m)-(o), we plot the RSD parameter versus the reciprocal of F_{av} in case $d = 0.26\lambda_b$, $d = 0.33\lambda_b$ and $d = 0.4\lambda_b$. Note that distances higher than $0.5\lambda_b$ are not suitable as they do not allow an accurate control of the field intensity.

According to the proposed procedure, $\phi_1 \in [0, \pi/3]$ are the optimal phase shifts leading to an appropriate interference while the ones in proximity of π can be discarded. Then, the corresponding field amplitude distributions (shown in Figure 3) are the ideal ones to be eventually considered within a field synthesis optimization procedure.

B. CASE STUDY 2: FOUR CONTROL POINTS

The scenario under test is depicted in Figures 4(a). The control points are located at distances of about $d_{02} = 0.42\lambda_b$ and $d_{13} = 0.32\lambda_b$. Both midpoints are at $(0, 0)$ m, while the reference point is the one in $(0, 0.21\lambda_b)$. The ROI is represented by the yellow area in Figure 4(a).

According to step 3 in Figure 2, in order to explore all the possible combinations of phase shifts, M = 20 values

for each ϕ_i have been uniformly sampled in the interval $[0, 2\pi[$. Then, the total number of possible combinations is $M^{L-1} = 8000$.

The RSD parameter versus the reciprocal of F_{av} is plotted in Figure 4(e). Each circle represents a pair of values (RSD, $1/F_{av}$) corresponding to one of the 8000 phase shifts combinations. As in case of two control points, convenient combinations exist which corresponds to the circles in the region close to the origin of the coordinates system. We consider the region such that $RSD \leq 0.15$ and $1/F_{av} \leq 3.8$. Then, the number of convenient combinations to be eventually considered for the problem at hand is drastically reduced to 216.

A combination ensuring a good tradeoff is the combination (0, 0, 0) and the corresponding auxiliary field distribution is shown in Figure 4(b). Figure 4(c) shows instead the auxiliary field distribution corresponding to a phase shifts combination giving a minimum RSD. Finally, Figure 4(d) shows the auxiliary field distribution corresponding to a phase shifts combination giving a maximum RSD.

In Section VI, the effectiveness of the convenient phase shifts suggested in case of two and four control points by the above analysis based on the auxiliary field model (3) are tested in the relevant case of MRI shimming.

C. A CHALLENGING SHAPING PROBLEM: MRI SHIMMING

One of the main challenges for MRI at high and ultra-high fields is the possibly significant inhomogeneity in the RF transmit magnetic field [7], [15]. Indeed, high frequency can cause electromagnetic field spatial variations which significantly degrade the image quality.

Different RF shimming approaches have been proposed in literature, which can be classified into two main categories: passive and active ones [7], [15]–[22]. The first category commonly uses high-permittivity materials put close to the ROI to vary the spatial distribution of the magnetic field, improve field homogeneity and enhance signal noise ratio [16]–[19]. For instance, in [17] a series of electromagnetic simulations have been performed to observe and quantify the improvements achieved using higher permittivity materials between the RF coil and the patient. In [16] dielectric shimming is formulated as an electromagnetic scattering problem using integral equations.

On the other hand, in the active shimming techniques, the RF field inhomogeneity can be addressed by using multi-element transmit coils [20]–[22]. These techniques can be also optimized to reduce global SAR, since interferences between the electric fields from multiple transmit coils can result in amplifications of local SAR which are difficult to predict [21]–[22]. For instance, in [20] a synthesis procedure has been proposed for the RF shimming able to take contemporaneously into account all constraints regarding homogeneity, strength and polarization. However, this method could be trapped into sub-optimal solutions and enforce the field homogeneity in the whole investigation domain, without the possibility to restrict this requirement to a subdomain.

In this section, the auxiliary field model for intensity shaping proposed in Section III are exploited for the challenging MRI shimming case. In particular, the RF shimming is set up by exploiting one or more control points located in the ROI (as in *multi-control points*-based approaches [9]–[10]) and by taking into account the constraints regarding SAR levels and polarization purity.

To this end, we consider a birdcage coil made up of N conductors, each one fed by a different current I_n (with $n = 1, \ldots, N$). Our goal is to find the complex excitations I_n that produce in the ROI the desired field $B_1^+(\underline{r})$, that is the right-hand circular polarization of the RF magnetic field. Then, the optimization problem can be formulated as follows:

"Determine the optimal set of complex excitations coefficients I_n such to produce a uniform and sufficient intense B_1^+ field, while ensuring polarization purity and SAR limits in the overall D".

Then, from a mathematical point of view, the RF shimming problem can be cast as follows:

$$\max_{I_n} \quad \mathcal{R}\{B_1^+(\underline{r}_{t_o}, I_n)\}, \tag{5a}$$

$$\text{subject to} \quad \mathfrak{I}\{B_1^+(\underline{r}_{t_0}, I_n)\} = 0, \tag{5b}$$

$$\mathcal{R}\{B_1^+(\underline{r}_{t_i}, I_n)\} = \mathcal{R}\{B_1^+(\underline{r}_{t_0}, I_n)\} \cos\Delta\phi_i, \tag{5c}$$

$$\mathfrak{I}\{B_1^+(\underline{r}_{t_i}, I_n)\} = \mathcal{R}\{B_1^+(\underline{r}_{t_0}, I_n)\} \sin\Delta\phi_i, \tag{5d}$$

$$SAR(\underline{r}, I_n) \leq 3.2 \frac{\text{W}}{\text{kg}} \qquad \underline{r} \in D, \tag{5e}$$

$$|B_1^-(\underline{r}, I_n)|^2 \leq \frac{1}{2}|B_{1,initial}^+(\underline{r}, I_n)|^2 \quad \underline{r} \in D, \tag{5f}$$

$$|B_1^+(\underline{r}, I_n)|^2 \leq |B_{1\,des}^+|^2 \qquad \underline{r} \in \Sigma, \tag{5g}$$

wherein $\mathcal{R}\{\cdot\}$ and $\mathfrak{I}\{\cdot\}$ are the real and the imaginary parts of the corresponding argument, respectively. $SAR = \frac{\sigma(r)}{\rho(r)}|E(\underline{r})|^2$ and ρ is the mass density of tissues. B_1^- is the undesired left-hand polarization of the RF magnetic field, $B_{1,initial}^+(\underline{r}, I_n)$ is the spatial distribution of B_1^+ in a standard coil, according to [20], and Σ is the part of D which does not contain the ROI. Finally, $\Delta\phi_i \in [0, 2\pi[$ are auxiliary variables indicating the phase shifts between the field in $\underline{r}_{t_0}$ and $\underline{r}_{t_i}$. Note that whatever the values of the auxiliary variables $\Delta\phi_i$, constraints (5.b) and (5.c) allow to enforce equality of the field amplitude at the control points.

In problem (5) the magnetic field B_1^+ in $\underline{r}_{t_0}$ is assumed real by simply changing the overall phase reference. Note that variables $\Delta\phi_i$ are different from the variables ϕ_i in the auxiliary model (3). In fact, in model (3) the phase of $F_{aux}(\underline{r}_{t_0})$ can be different from zero, while in problem (5) the actual field B_1^+ is enforced to be real in $\underline{r}_{t_0}$. Second, and more important, variables $\Delta\phi_i$ are the phase shifts amongst the total fields B_1^+ at the control points, while variables ϕ_i are the phase shifts amongst the different Bessel functions contributions.

In problem (5), constraint (5.e) limits the SAR levels everywhere according to [20], [23]. Constraint (5.f) regards the field polarization, which is enforced to remain close enough to the desired right-hand one [20]. Finally, by means of constraint (5.g), the square amplitude of B_1^+ is enforced to lie under a specific upper bound $B_{1\,des}^+$ in the region Σ.

For any fixed frequency and $\Delta\phi_i$ value, the MRI shimming problem (5) is recast as the maximization of a linear function in a convex set, which corresponds to a convex programming (CP) problem [9], [10]. Then, the globally optimal solution of the overall optimization problem can be a posteriori determined by exploring all the different possible combinations for $\Delta\phi_i$, solving then the corresponding CP problem and finally looking into the values of the cost function or other suitable performance indicators depending on the application at hand [9]–[12]. Alternatively, in a more convenient fashion, a nested optimization procedure where the external global optimization acts on the field phase shifts whereas the internal convex optimization acts instead on excitations can be also exploited [11]. Note that some preliminary analysis and results for MRI shimming via purely enumerative optimization in case of simplified and homogeneous brain models have been shown in the conference paper [24] by the same authors.

If the optimal phase shifts were a priori known, just a single CP problem would have to be solved. Unfortunately, such an information is not generally available. On the other side, which is a relevant circumstance, exploitation of the proposed auxiliary model (3) can be profitably exploited to off-line discard non-convenient phase shifts values in *multi-control points*-based procedures. In fact, the knowledge of some optimal sets of $\{\phi_i\}$ values implies a straightforward computation of the corresponding $\{\Delta\phi_i\}$, which are instead
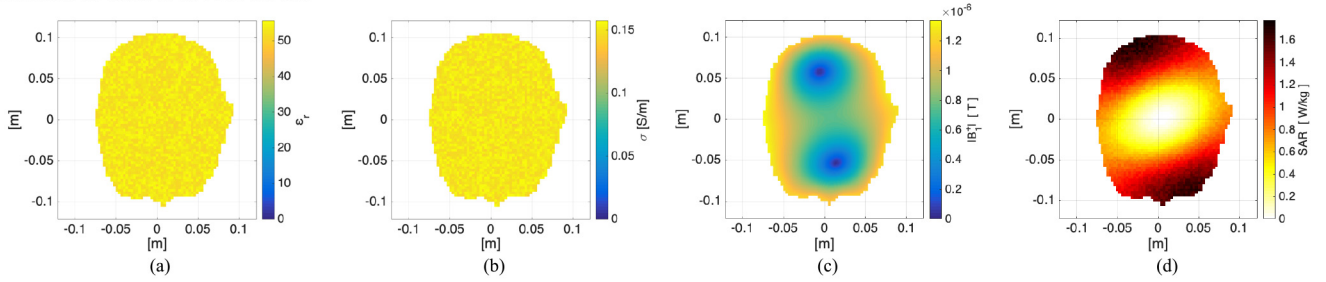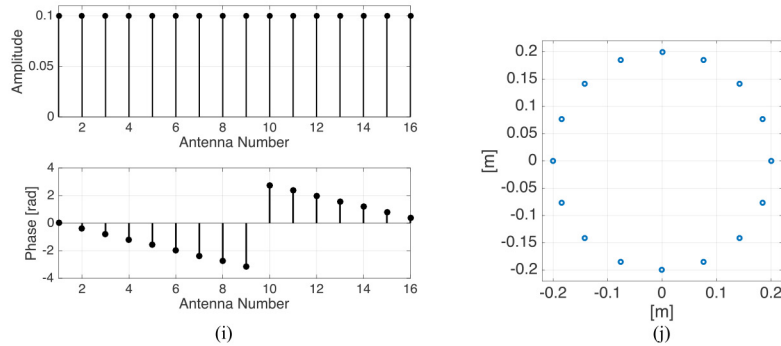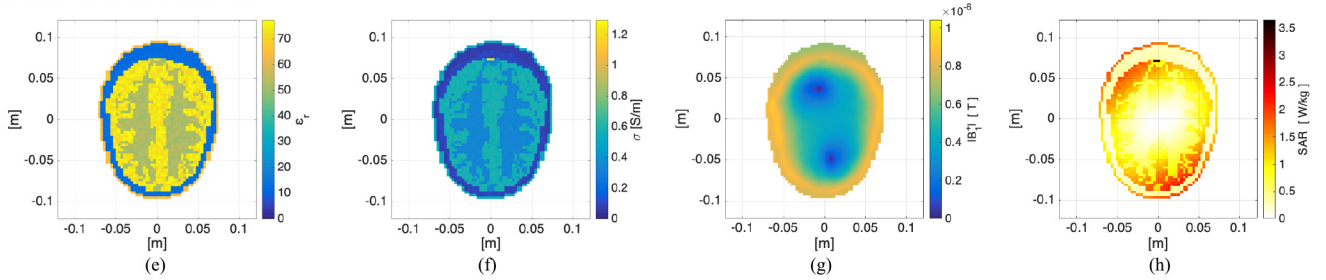
HOMOGENEOUS HEAD PHANTOM

REALISTIC HEAD PHANTOM

FIGURE 5. MRI shimming against 2D head phantoms: relative permittivity (a), (e) and electrical conductivity (b), (f) maps. Spatial distributions of the amplitude of the magnetic field B_1^+ [T] (c), (g) and SAR [W/kg] (d), (h) corresponding to a standard coil configuration. Amplitude and phase (i) of the standard excitation coefficients. (j) Positions of the antennas of the circular array schematizing the birdcage coil.

the actual phase shifts of the B_1^+ field between the field in $\underline{r}_{t_i}$ and in the reference point $\underline{r}_{t_0}$[2]. Then, one can go to the shaping problem of interest (5) and solve it just for the more convenient $\{\Delta\phi_i\}$ combinations as resulting from step 5 in Figure 2. This restriction of the $\{\Delta\phi_i\}$ combinations involves a drastic reduction of the computational burden. Notably, such a reduction is more and more pronounced with an increasing number of control points, and hence in cases of large ROI and/or 3D geometry.

In the following section, the shimming approach (5) and the analysis reported in Section IV is tested against two 2D head phantoms. $B_{1\,des}^+$ is set equal to 1/3 of the infinite norm of the amplitude of the field $B_{1,initial}^+(\underline{r}, I_n)$ [20], while Σ is assumed to be the region outside the brain support.

V. NUMERICAL ANALYSIS IN THE MRI SHIMMING CASE
Two different 2D head phantoms have been considered for the analysis. The first one has been obtained by considering the morphological information gathered from a 3D

---
2. In particular, one can determine $\Delta\phi_i$ as $\phi_i - \angle F_{aux}(\underline{r}_{t_0}, \{\phi_i\})$.

high-resolution voxel-based anthropomorphic phantom [25] and by defining the electromagnetic properties according to IT'IS foundation database [26]. A transverse slice has been considered and enclosed within a square domain D, discretized as in Section III. In the second phantom, the head has been instead modeled as a homogeneous medium with electrical properties set equal to the average value of the ones of the brain tissues, that is with relative permittivity of 53 and electrical conductivity 0.15.

Figures 5(a)-(b) and 5(e)-(f) depict respectively the relative permittivity and the electrical conductivity distributions of both scenarios.

In order to simulate an MRI scanner, the birdcage structure has been schematized as a circular antenna array of radius $0.2m$, in accordance with the realistic size of common birdcage coil adopted in clinic and located around the head phantom with 16 antennas evenly spaced [20] (see Figure 5(j)). Air has been assumed to be the background medium. For comparison, the coefficients I_{n_0} corresponding to the standard design of the birdcage coil configuration have been considered according to [20]. Finally, the considered
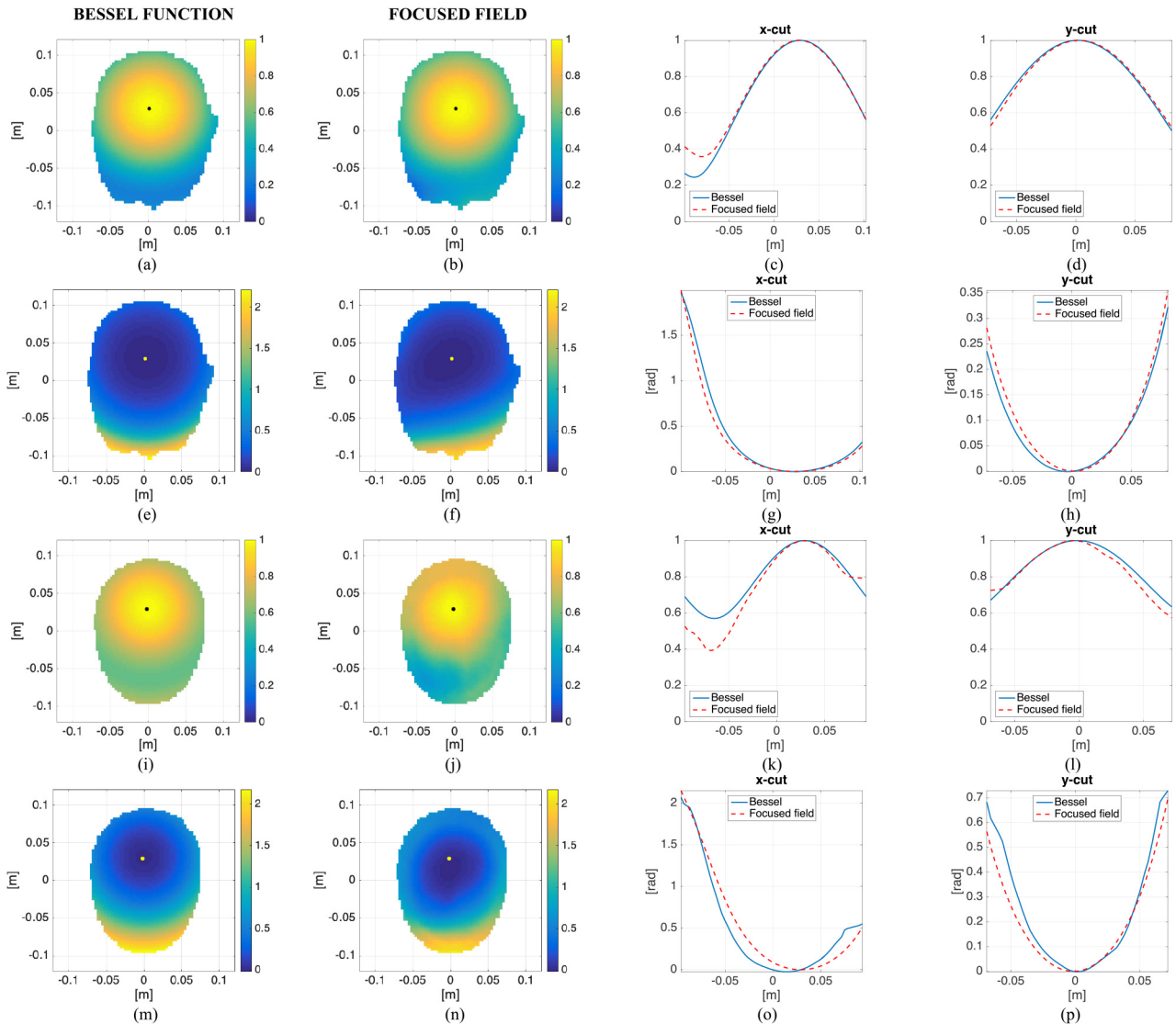
FIGURE 6. MRI shimming against 2D head phantoms. (a)-(h) Homogeneous and (i)-(p) realistic head phantoms. Amplitudes distributions of (a), (i) the Bessel function of zero order and (b), (j) the field focused via problem (5) in case of a single control point located in (0, 0.029 m). Corresponding cut views along (c), (k) x-axis at y = 0.029 and (d), (l) y-axis at x = 0 (zoomed in on the brain support). Phase distributions of (e), (m) the Bessel function of zero order and (f), (n) the field focused via problem (5). Corresponding cut views along (g), (o) x-axis at y = 0.029 and (h), (p) y-axis at x = 0 (zoomed in on the brain support). The continuous lines correspond to the Bessel function of zero order, while the dashed lines correspond to the focused field.

Larmor frequency is 128 MHz, which corresponds to a static field $B_0 = 3T$.

In Figures 5(c) and (d) and 5(g) and (h), the spatial distributions of the B_1^+ field and the SAR corresponding to the standard coil configuration are shown, respectively, for the two head phantoms, while in Figure 5(i) the magnitude and phase of the standard array excitation coefficients $[I_{n_0}]$ are reported.

As first step, a single control point located at (0, 0.029 m) has been considered and the corresponding focusing problem has been solved. In both cases, for the evaluation of the argument of the Bessel function in the field approximation (3), the average of both the relative permittivity and electrical conductivity have been considered, i.e., about 53 and 0.15, respectively. The amplitudes and phases of the Bessel function and the actual focused magnetic field are shown in Figure 6 for both head phantoms. As it can be seen, the spatial distribution of B_1^+ can be well approximated within the head support by the Bessel function of zero order, which means that consideration of just the first term of expansion (2) is suitable for understanding expected behaviors in term of $\{\phi_i\}$ (and hence $\{\Delta\phi_i\}$). Notably, the auxiliary model (3) can still be used notwithstanding the inhomogeneity of the scenario.

A. CASE STUDY 1: TWO CONTROL POINTS

The control points have been located as in Figure 3(a) at $d = 0.27\lambda_m$, where λ_m is the wavelength refers to the mean of the brain electrical properties. The chosen ROI is represented by the yellow ellipse in Figure 7(a) and 8(a), respectively for the homogeneous and realistic head phantoms.
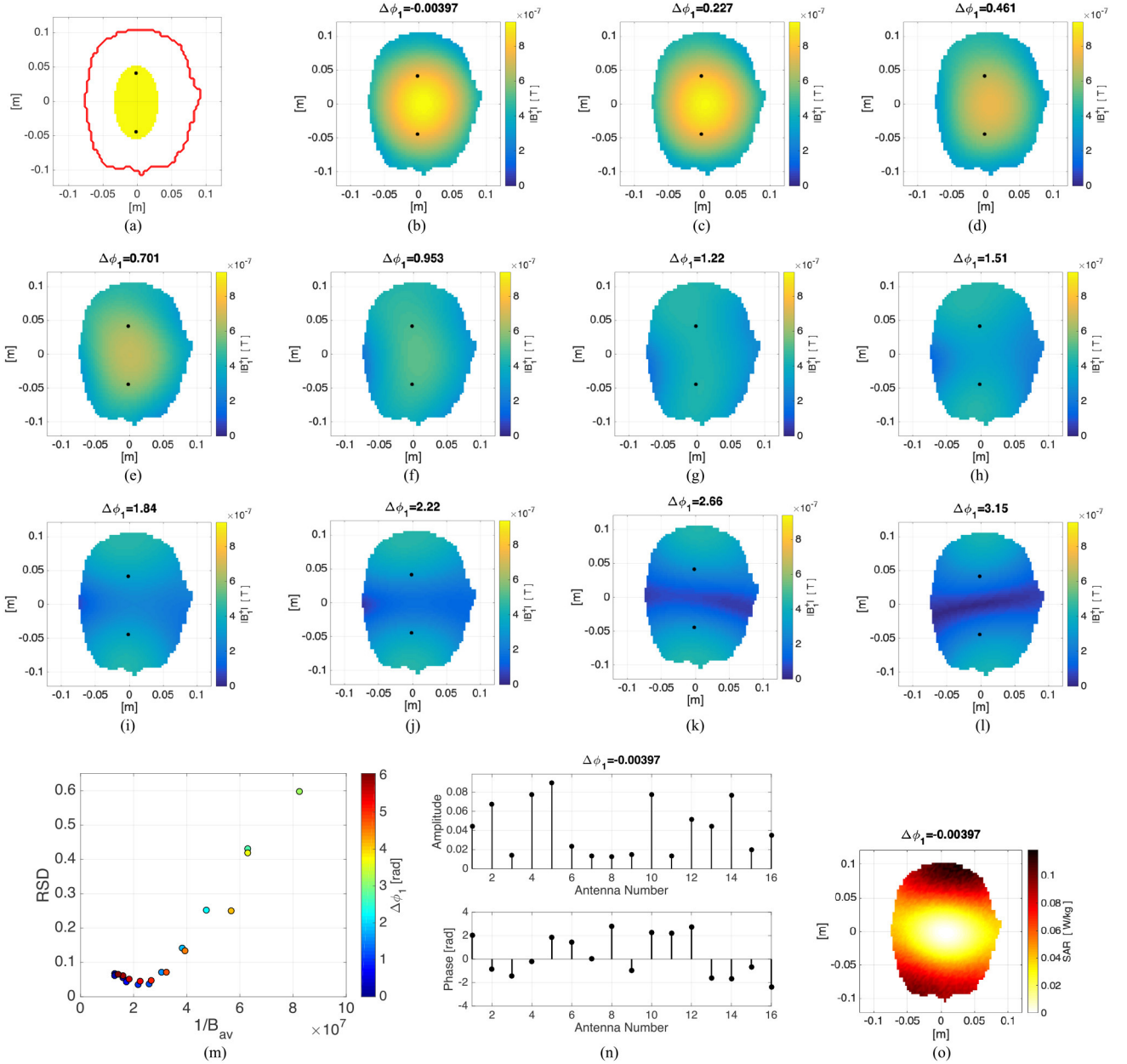
FIGURE 7. MRI shimming against 2D head phantoms. CASE STUDY 1: Homogeneous head phantom. The ROI is the yellow area (a), while the control points are superimposed as black points. (b)-(l) Spatial amplitude distributions of the magnetic field B_1^+ [T] for different value of phase shifts in [0,π]. (m) RSD versus the reciprocal of B_{av} [T]. Each circle represents a pair of values (RSD, $1/B_{av}$) corresponding to a given phase shift. The different colors correspond to a value of $\Delta\phi_1$. (n) Amplitude and phase of the optimal excitation coefficients and (o) SAR [W/kg] spatial distribution corresponding to the optimal $\Delta\phi_1$.

In order to check the usefulness of the analysis reported in Section IV-A, all the M = 20 values of the phase shift $\Delta\phi_1$ have been considered in the solution of problem (5). In case of homogeneous head phantoms, the spatial distributions of the B_1^+ field corresponding to the first 11 $\Delta\phi_1$ values are shown in Figures 7(b)-(l) and 8(b)-(l). According to Section IV-A, just a few values $\Delta\phi_1$ values, evaluated as $\phi_1 - \angle F_{aux}(\underline{r}_{t_0}, \phi_1)$, allow to ensure both a uniform and maximum spatial distribution of the field intensity.

To better handle the underlying trade-off, the RSD parameters versus the reciprocals of B_{av}, i.e., the average value of the

B_1^+ intensity, are shown in Figures 7(m) and 8(m)[3]. Notably, the same qualitative behavior as in Figure 3(m) is obtained. Then, the proposed off-line analysis of the auxiliary model can be assumed to effectively predict the convenient and the non-convenient field interferences, even if the biological scenario under test is significantly heterogeneous.

As expected, this procedure gives significant advantages in terms of computational complexity, as just 4 CP problems

---

3. In such graphs, the last 11 exemplementary angles within]π, 2π[are also shown as they can have slightly different performance due to the heterogeneity of the scenario under test.
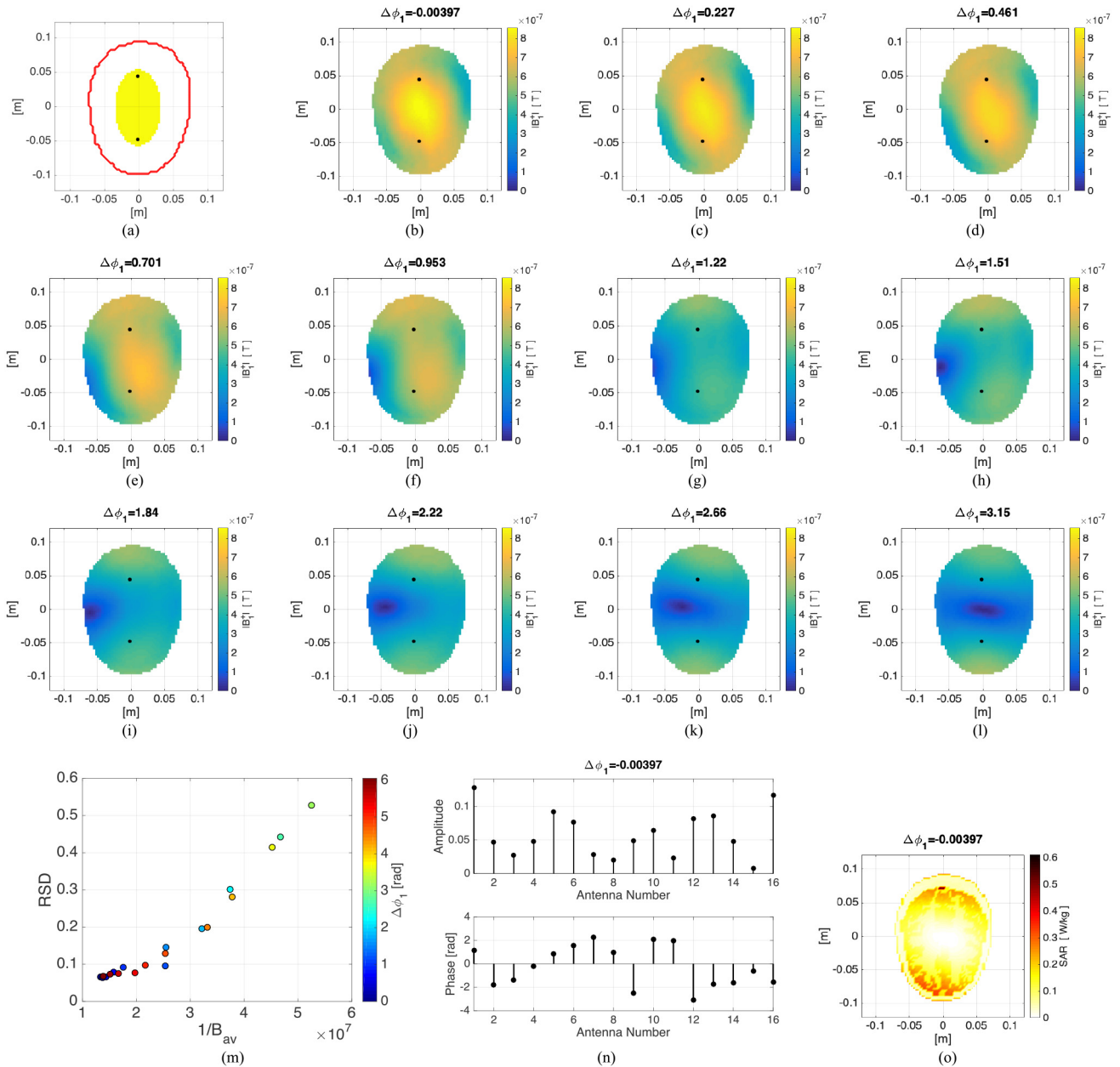
FIGURE 8. MRI shimming against 2D head phantoms. CASE STUDY 1: Realistic head phantom. The ROI is the yellow area (a), while the control points are superimposed as black points. (b)-(l) Spatial amplitude distributions of the magnetic field B_1^+ [T] for different value of phase shifts in $[0,\pi]$. (m) RSD versus the reciprocal of B_{av} [T]. Each circle represents a pair of values (RSD, $1/B_{av}$) corresponding to a given phase shift. The different colors correspond to a value of $\Delta\phi_1$. (n) Amplitude and phase of the optimal excitation coefficients and (o) SAR [W/kg] spatial distribution corresponding to the optimal $\Delta\phi_1$.

need to be solved by exploiting the outcomes of the auxiliary model analysis, whereas the enumerative solution of problem (5) requires the solution of 20 CP problems. It is important to note that the time saving is anyway much larger than the approximatively one order of magnitude, from 20 to 4 CP problems. In fact, some of the original 20 optimization problems and specifically, those corresponding to the non-convenient $\Delta\phi_1$ values are severely ill-conditioned, so that their solution can be very slow. Obviously, computational advantages are more and more pronounced as M and L increase (see next subsection) and in 3D geometry.

Please note that the RSD of B_1^+ corresponding to the standard choice of the excitations (see [20]) is 0.33, while by means of the proposed shimming procedure, the optimal phase shift can ensure an RSD much lower than 0.1. This means that a more uniform B_1^+ field has been now obtained respect to the standard distribution. This final RSD is the same as the one obtained by performing an enumerative optimization as in [24].

The optimal phase shift for the considered choice of control points correspond to $\Delta\phi_1 \sim 0$ (see Figures 7 and 8) as it also ensures the best field amplitude distribution.
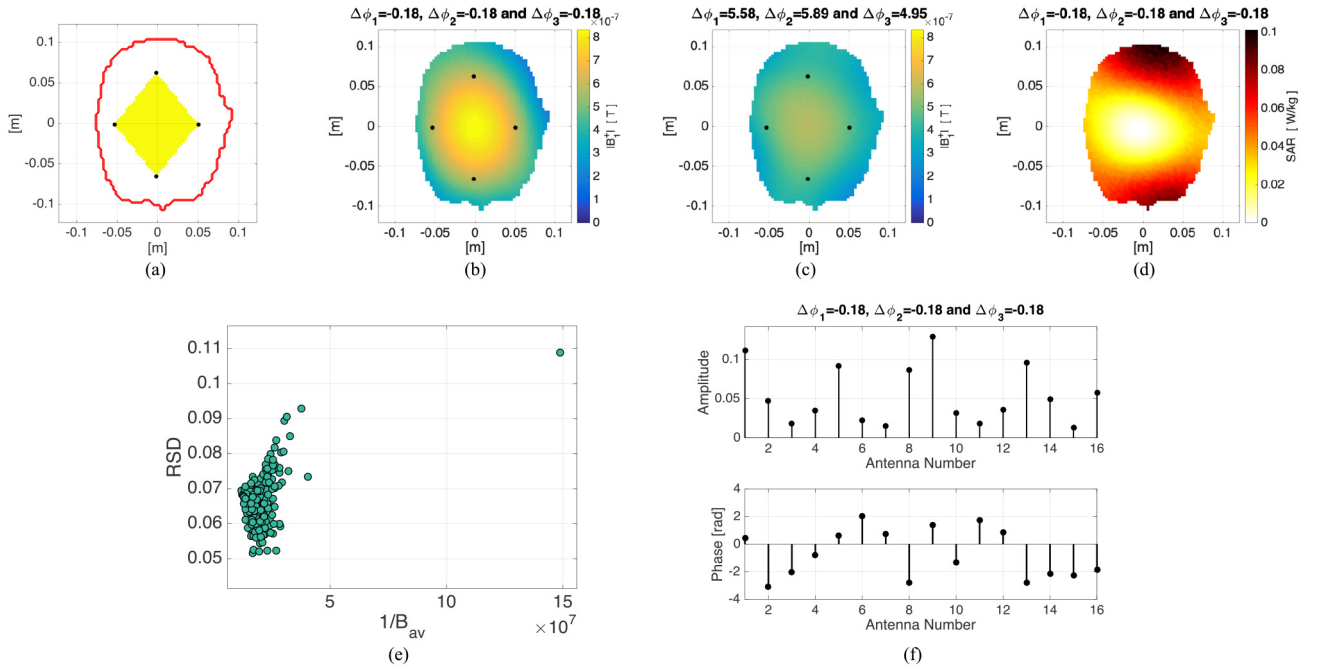
FIGURE 9. MRI shimming against 2D head phantoms. CASE STUDY 2: Homogeneous head phantom. The ROI is the yellow area (a), while the control points are superimposed as black points. Spatial amplitude distributions of the magnetic field B_1^+ [T] in case of (b) good tradeoff between RSD and maximum field intensity in the ROI and (c) minimum RSD. (d) SAR [W/kg] spatial distribution corresponding to (b). (e) RSD versus the reciprocal of B_{av} [T]. Each green circle represents a pair of values (RSD, $1/B_{av}$) corresponding to a given combination of phase shifts. (f) Amplitude and phase of the optimal excitation coefficients corresponding to (b).

Figures 7(n) and 8(n) give the corresponding optimal amplitudes and phase of the complex excitations I_n for both the homogenous and the realistic head phantoms. Note that the procedure also allows a satisfactory control of SAR levels into the ROI, as shown in Figures 7(o) and 8(o).

B. CASE STUDY 2: FOUR CONTROL POINTS
The control points have been located as in Figure 4(a) at a distance of $d_{02} = 0.42\lambda_m$ and $d_{13} = 0.32\lambda_m$ (see Figures 9(a) and 10(a)). Both midpoints are at (0,0) m. As a consequence, the already available analysis of Section IV-B can be applied. If all the possible combinations were considered for problem (5), with M = 20 values for each ϕ_i, 8000 convex problems should be solved, which would mean a very expensive and time-consuming procedure. However, results in Section IV-B have shown that some combinations are not convenient for the application at hand. Then, in the following, we have considered only those combinations that ensure a good compromise between uniform spatial distribution and maximum of the field, that are the 216 combinations in the region $RSD \le 0.15$ and $1/F_{av} \le 3.8$ in Figure 4(e).

The RSD parameters versus the reciprocals of B_{av} is shown in Figures 9(e) and 10(e). The optimal phase shift combinations are $\Delta\phi_1 = -0.18$, $\Delta\phi_2 = -0.18$ and $\Delta\phi_3 = -0.18$ and $\Delta\phi_1 = -0.263, \Delta\phi_2 = 5.71$ and $\Delta\phi_3 = -0.263$ respectively for the homogeneous and realistic phantoms. Indeed, they ensure the best field distributions. The optimal field distributions are shown in Figures 9(b) and 10(b), while the ones corresponding to the minimum RSD are reported in

Figures 9(c) and 10(c). Note that the RSD of B_1^+ evaluated for the standard choice of excitations [20] is 0.34, while, by means of the proposed shimming procedure, the RSD is lower than 0.08. This final RSD is the same as to the one obtained by performing an enumerative optimization as in [24], so that also in this case the achieved time saving does not imply a worsening of performances.

Figures 9(f) and 10(f) give the corresponding optimal amplitudes and phases of the complex excitations I_n of the N conductors, while the reached SAR levels into the brain are shown in Figures 9(d) and 10(d). The above results, and other cases not shown herein for the sake of brevity, demonstrate the feasibility and the accuracy of the proposed auxiliary model in predicting the field interferences within the ROI and the optimal phase shifts combinations to be used in the solution of the original problem (5). Moreover, the off-line analysis of the auxiliary model (3) has allowed to obtain the optimal I_n without the solution of a very high number of CP problems and, thus, with a reduced computational burden related to the *multi-control points*-based approaches. As a matter of fact, in case of four control points we have a reduction factor of about 40 of the number of CP problems, resulting in an even larger factor in terms of overall computational time. In order to emphasize such reduction, two metrics are adopted and reported in Table 1, that are the numbers of involved CP problems and the computational time for the two cases wherein the proposed auxiliary model or the standard enumerative strategy in [10], [11], [24] are adopted, respectively.
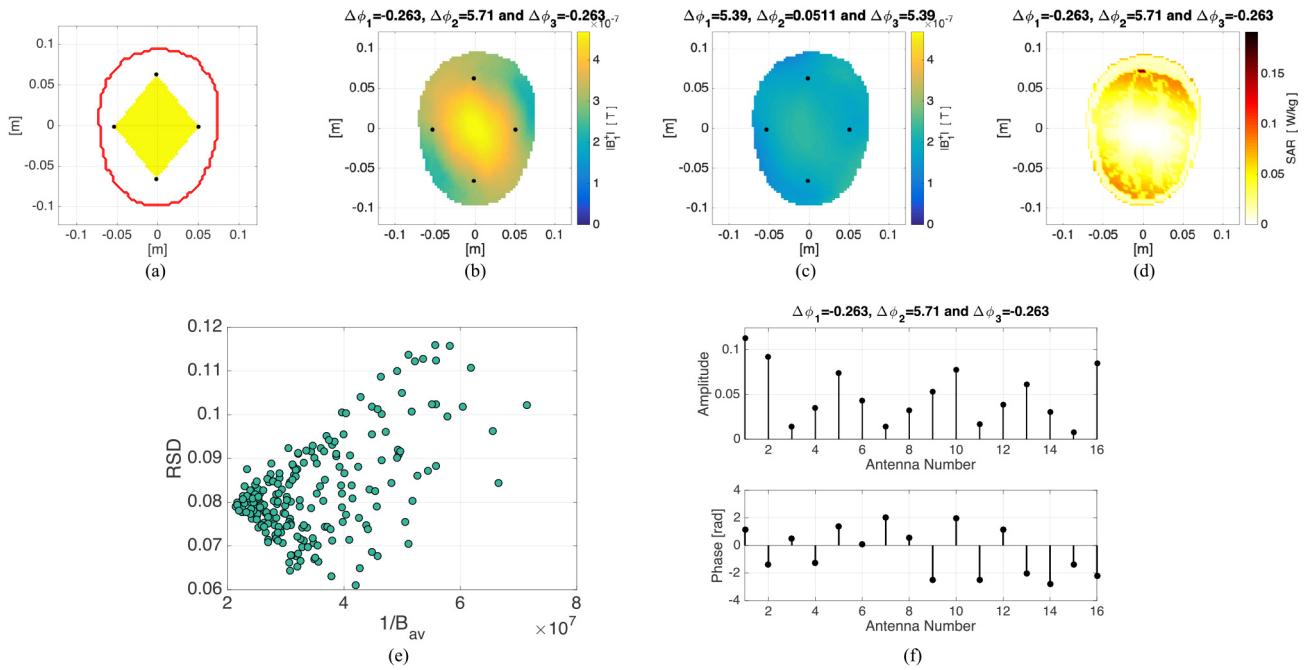
FIGURE 10. MRI shimming against 2D head phantoms. CASE STUDY 2: Realistic head phantom. The ROI is the yellow area (a), while the control points are superimposed as black points. Spatial amplitude distributions of the magnetic field B_1^+ [T] in case of (b) good tradeoff between RSD and maximum field intensity in the ROI and (c) minimum RSD. (d) SAR [W/kg] spatial distribution corresponding to (b). (e) RSD versus the reciprocal of B_{av} [T]. Each green circle represents a pair of values (RSD, $1/B_{av}$) corresponding to a given combination of phase shifts. (f) Amplitude and phase of the optimal excitation coefficients corresponding to (b).

TABLE 1. Advantages in term of computational burden: number of CP problems to be solved and computational time.

	# CP problems		Computational time	
L	2	4	2	4
proposed approach	4	216	~3 min	~5 h
enumerative approach [24]	20	8000	~26 min	~570 h

VI. CONCLUSION

In this paper, an auxiliary model has been proposed for shaping the field intensity distribution in a given target region, supporting the design of complex excitations feeding a fixed geometry array.

This physics inspired model allows to understand the possible spatial field distributions by analyzing the interferences between canonical solutions for the induced total field in the ROI, that are zero order Bessel functions. Such analysis allows to discard the non-convenient interferences depending on the application at hand. Then, it allows a significant reduction of computational resources by ensuring the same performance. Obviously, the analysis of model (3) becomes more and more demanding in case of a larger and larger number of control points. However, by taking advantage from the peaked behavior of the elementary bricks, a possible strategy for the case of very many control points could be that of starting from a portion of the actual ROI, which implies a reduced number of control points. Then, after some selections of the first phase shifts of interest, one can increase the portion of interest, and hence the number of control points. In such a way, one can avoid testing all the possible combinations, thus limiting the computational burden.

While relevant in several applications, the usefulness of the proposed auxiliary model has been tested in the case of MRI shimming. The numerical analysis against a realistic head phantom has outlined that the proposed auxiliary model can be effective also in case of non-homogenous medium. Moreover, consideration of a set of optimal phase shifts combinations based on the proposed auxiliary model, rather than selecting a unique optimal phase shift combination, has to be preferred especially in case of a number of control points higher than 2. In fact, such a choice allows to compensate possible small variations of the field distribution due to the heterogeneous scenario under test, and to better tailor the results to the application at hand.

Future work will be devoted at testing the procedure in other relevant applications, such as hyperthermia treatment planning and array synthesis for telecommunications, as well as to cases where the overall field intensity rather than the amplitude of a single component is of interest [27]. Furthermore, the extension of the rationale underlying the proposed auxiliary model will be addressed in the more challenging 3D vectorial scenario, wherein its features would become even more attractive.

APPENDIX

Consider two control points $\underline{r}_{t_0}$ and $\underline{r}_{t_1}$ located at distance d in a lossless and homogeneous ROI, characterized by a wave

number k_m. Then, the auxiliary model (3) can be simplified as follows:

$$F_{aux}(\underline{r}) = J_0\big(k_m|\underline{r} - \underline{r}_{t_0}|\big) + J_0\big(k_m|\underline{r} - \underline{r}_{t_1}|\big)e^{j\phi_1} \quad \text{(A.1)}$$

In such a simple case, one can analytically determine the values of ϕ_1 such that the field amplitudes are the same at $\underline{r}_{t_0}$, $\underline{r}_{t_1}$ and at midway. Indeed, by evaluating the amplitudes of $F_{aux}(\underline{r})$ at these points, that are:

$$\left|F_{aux}\big(\underline{r}_{t_0}\big)\right| = \left|1 + J_0(k_m d)e^{j\phi_1}\right| \quad \text{(A.2a)}$$

$$\left|F_{aux}\big(\underline{r}_{t_1}\big)\right| = \left|J_0(k_m d) + e^{j\phi_1}\right| \quad \text{(A.2b)}$$

$$\left|F_{aux}\left(\frac{\underline{r}_{t_1} + \underline{r}_{t_2}}{2}\right)\right| = \left|J_0\left(\frac{k_m d}{2}\right) + J_0\left(\frac{k_m d}{2}\right)e^{j\phi_1}\right| \quad \text{(A.2c)}$$

and by imposing the three right hand members to be equal to each other, one can derive for the case of a lossless medium the ϕ_1 values such to obtain a uniform field in the ROI, i.e.:

$$\phi_1 = \arccos\left\{\frac{1 + [J_0(k_m d)]^2 - 2\left[J_0\left(\frac{k_m d}{2}\right)\right]^2}{2\left[J_0\left(\frac{k_m d}{2}\right)\right]^2 - 2J_0(k_m d)}\right\} \quad \text{(A.3)}$$

REFERENCES

[1] P. Angeletti and J. L. Cubillos, "Traffic balancing multibeam antennas for communication satellites," *IEEE Trans. Antennas Propag.*, vol. 69, no. 12, pp. 8291–8303, Dec. 2021.

[2] M. Mosalanejad, S. Brebels, C. Soens, I. Ocket, and G. A. E. Vandenbosch, "Millimeter wave cavity backed microstrip antenna array for 79 GHz radar applications," *Progr. Electromagn. Res.*, vol. 158, pp. 89–98, Jan. 2017.

[3] R. G. Ayestarán, G. León, M. R. Pino, and P. Nepa, "Wireless power transfer through simultaneous near-field focusing and far-field synthesis," *IEEE Trans. Antennas Propag.*, vol. 67, no. 8, pp. 5623–5633, Aug. 2019.

[4] P. Nepa and A. Buffi, "Near-field-focused microwave antennas: Near-field shaping and implementation," *IEEE Antennas Propag. Mag.*, vol. 59, pp. 42–53, 2017.

[5] S. Costanzo and G. D. Massa, "Near-field focusing technique for enhanced through-the-wall radar," in *Proc. 11th Eur. Conf. Antennas Propag. (EUCAP)*, 2017, pp. 1716–1717, doi: 10.23919/EuCAP.2017.7928508.

[6] M. M. Paulides, G. M. Verduijn, and N. Van Holthe, "Status quo and directions in deep head and neck hyperthermia," *Radiat. Oncol.*, vol. 11, no. 1, p. 21, 2016.

[7] W. Mao, M. B. Simth, and C. M. Collins, "Exploring the limits of RF shimming for high field MRI of the human head," *Magn. Res. Med.*, vol. 56, no. 4, pp. 918–922, 2006.

[8] J. L. Thomas, F. Wu, and M. Fink, "Time reversal focusing applied to lithotripsy," *Ultrasonic Imag.*, vol. 18, no. 2, pp. 106–121, 1996.

[9] G. G. Bellizzi, D. A. M. Iero, L. Crocco, and T. Isernia, "Three-dimensional field intensity shaping: The scalar case," *IEEE Antennas Wireless Propag. Lett.*, vol. 17, no. 3, pp. 360–363, Mar. 2018.

[10] G. G. Bellizzi, M. T. Bevacqua, L. Crocco, and T. Isernia, "3-D field intensity shaping via optimized multi-target time reversal," *IEEE Trans. Antennas Propag.*, vol. 66, no. 8, pp. 4380–4385, Aug. 2018.

[11] G. M. Battaglia, A. F. Morabito, G. Sorbello, and T. Isernia, "Mask-constrained power synthesis of large and arbitrary arrays as a few-samples global optimization," *Progr. Electromagn. Res. C*, vol. 98, pp. 69–81, Jan. 2020.

[12] G. G. Bellizzi, T. Drizdal, G. C. van Rhoon, L. Crocco, T. Isernia, and M. M. Paulides, "Advances in multi-target FOCO for hyperthermia treatment planning: A robustness assessment," in *Proc. 12th Eur. Conf. Antennas Propag. (EuCAP)*, 2018, pp. 1–4, doi: 10.1049/cp.2018.0930.

[13] P. Woodward and J. Lawson, "The theoretical precision with which an arbitrary radiation-pattern May be obtained from a source of finite size," *J. Inst. Elect. Eng. III Radio Commun. Eng.*, vol. 95, no. 37, pp. 363–370, 1948.

[14] D. S. Jones, *Acoustic and Electromagnetic Waves*. Oxford, U.K.: Clarendon, 1986.

[15] W. M. Brink, V. Gulani, and A. G. Webb, "Clinical applications of dual-channel transmit MRI: A review," *J. Magn. Reson. Imag.*, vol. 42, no. 4, pp. 855–869, 2015.

[16] W. M. Brink, R. F. Remis, and A. G. Webb, "A theoretical approach based on electromagnetic scattering for analysing dielectric shimming in high-field MRI," *Magn. Reson. Med.*, vol. 75, no. 5, pp. 2185–2194, 2016.

[17] R. Schmidt and A. G. Webb, "Improvements in RF shimming in high field mri using high permittivity materials with low order pre-fractal geometries," *IEEE Trans. Med. Imag.*, vol. 35, no. 8, pp. 1837–1844, Aug. 2016.

[18] G. Ruello and R. Lattanzi, "A physical framework to interpret the effects of high permittivity materials on radiofrequency coil performance in magnetic resonance imaging," *IEEE Trans. Biomed. Eng.*, early access, Apr. 7, 2022, doi: 10.1109/TBME.2022.3165763.

[19] G. G. Haemer *et al.*, "Approaching ultimate intrinsic specific absorption rate in radiofrequency shimming using high-permittivity materials at 7 Tesla," *Magn. Reson. Med.*, vol. 80, no. 1, pp. 391–399, 2018.

[20] E. A. Attardo, T. Isernia, and G. Vecchi, "Field synthesis in inhomogeneous media: Joint control of polarization, uniformity and SAR in MRI B1-field," *Progr. Electromagn. Res.*, vol. 118, pp. 355–377, Jul. 2011.

[21] B. Van den Bergen, C. A. Van den Berg, L. W. Bartels, and J. J. Lagendijk, "7 T body MRI: B1 shimming with simultaneous SAR reduction," *Phys. Med. Biol.*, vol. 52, no. 17, pp. 5429–41, 2007.

[22] I. P. Georgakis, A. G. Polimeridis, and R. Lattanzi, "A formalism to investigate the optimal transmit efficiency in radiofrequency shimming," *NMR Biomed.*, vol. 33, no. 11, 2020, Art. no. e4383.

[23] "Webstore." [Online]. Available: https://webstore.iec.ch/publication/22705(Accessed: Mar. 2022).

[24] S. Zumbo, M. T. Bevacqua, and T. Isernia, "MRI shimming via field intensity shaping," in *Proc. 12th Gen. Assembly Sci. Symp. Int. Union Radio Sci (URSI GASS)*, 2021, pp. 1–5, doi: 10.23919/URSIGASS51995.2021.9560209.

[25] I. Zubal, C. Harrell, E. Smith, Z. Rattner, G. Gindi, and P. Hoffer, "Computerized three-dimensional segmented human anatomy," *Med. Phys.*, vol. 21, no. 2, pp. 299–302, 1994.

[26] P. A. Hasgall *et al.*, "IT'IS database for thermal and electromagnetic parameters of biological tissues, version 3.0," 2015

[27] D. A. M. Iero, "Constrained power focusing in inhomogeneous media as a polarization optimization," *Int. J. Antennas Propag.*, vol. 2015, Oct. 2015, Art. no. 705819. [Online]. Available: https://doi.org/10.1155/2015/705819

SABRINA ZUMBO received the M.S. Laurea degree *(summa cum laude)* in electronic engineering from the Università Mediterranea di Reggio Calabria, Reggio di Calabria, Italy, in 2019, where she is currently pursuing the Ph.D. degree. Her research interests focus on the field of magnetic resonant imaging, in particular, radiofrequency field shimming and magnetic resonant imaging-based electrical property tomography.

TOMMASO ISERNIA (Fellow, IEEE) received the Laurea *(summa cum laude)* and Ph.D. degrees from the University of Naples Federico II, Naples, Italy.

He is currently a Full Professor of Electromagnetic Fields with the Università Mediterranea di Reggio Calabria, Reggio Calabria, Italy, where he serves as the Supervisor of the LEMMA Research Group and the Director of the Department of Information Engineering, Infrastructure and Sustainable Energy. He has served as a member of the Board of Administrators of Consorzio Nazionale Italiano per le Telecomunicazioni from 2013 to 2019, and he is currently a member of "Senato Accademico" of Università Mediterranea. His current research interests include inverse problems in electromagnetics, with particularly emphasis on phase retrieval, inverse scattering, and inverse source problems, as well as their applications to antenna synthesis and e.m. fields shaping for biomedical therapeutic applications.

Prof. Isernia was a recipient of the "G. Barzilai" Award from the Italian Electromagnetics Society in 1994.

MARTINA TERESA BEVACQUA (Member, IEEE) was born in Reggio Calabria, Italy, in 1988. She received the M.S. Laurea degree *(summa cum laude)* in electronic engineering and the Ph.D. degree in information engineering from the Università Mediterranea di Reggio Calabria, Italy, in July 2012 and May 2016, respectively.

She is currently working as an Assistant Professor with the Università Mediterranea di Reggio Calabria within a tenure track position. Her research activity mainly concerns electromagnetic inverse problems, with particular interest in: 1) inverse scattering problems from both a theoretical and applicative point of view and 2) field intensity focusing and shaping in nonhomogeneous and unknown scenario, in the framework of hyperthermia treatment planning, wireless power transfer and MRI shimming. He was the recipient of the "G. Barzilai" Award from the Italian Electromagnetics Society in 2014, while in March 2016, she received the Honorable Mention from IEEE-Antennas and Propagation Society (Central and Southern Italy Chapter) in the Best Student Member Paper competition. She was also the recipient of the URSI Young Scientist Award in 2018.